Surface & Coatings Technology xxx (xxxx) xxxx

Contents lists available at ScienceDirect

Surface & Coatings Technology

journal homepage: www.elsevier.com/locate/surfcoat

Characterization of yield criteria for zinc coated steel sheets using nano-indentation with knoop indenter

Tanmaya Mishra[a,*], Matthijn de Rooij[a], Meghshyam Shisode[b], Javad Hazrati[b], Dirk J. Schipper[a]

[a] Surface Technology and Tribology, Faculty of Engineering Technology, University of Twente, 7500 AE, Enschede, the Netherlands
[b] Nonlinear Solid Mechanics, Faculty of Engineering Technology, University of Twente, 7500 AE, Enschede, the Netherlands

ARTICLE INFO

Keywords:
Knoop indentation
Anisotropy
Yield locus
Zinc coating
Galvanized steel

ABSTRACT

An indentation based method to characterize the yield locus for steel sheets is developed and implemented. Knoop hardness based indentation experiments have been performed on the surface as well as on the cross sections of an uncoated steel sheet to obtain the corresponding yield locus in the deviatoric and plane-stress situation. Stress ratios following the indenter's geometry are used to plot the yield locus from indentation data. The stress ratios have been corrected for the anisotropy of the material by an optimization algorithm. Points are then plotted in the plane-stress plane using the corrected stress ratios, the strain increment vectors and indentation hardness data. The parameters for the Hill's quadratic yield criteria are obtained from the indentation data based on a curve fitted yield locus. The results obtained using nano-indentation have been compared with those obtained from the standard characterization tests for steel sheet and shown to have good agreement. The method is also applied to the yield locus characterization of zinc coatings on steel sheet for multi-scale modelling of friction in deep drawing.

1. Introduction

The plastic deformation (yielding) in metals results from shear stress which causes the formation and movement of dislocations at the slips systems in the crystals. The deformation modes in most crystals are directional resulting in anisotropic yielding of the metals on loading. In sheet metal forming processes like deep-drawing, metallic sheets are typically cold rolled *a priori* which induces a deformation texture in the sheet [1]. The textures, *i.e.* preferred orientations of crystals along direction of applied stress, are oriented along the rolling, transverse and normal directions. Hence most sheet metals exhibit anisotropic yielding which is described by a yield function and is represented by the corresponding yield surface in a three-dimensional principal stress space.

Of the available criteria, Hill's quadratic yield criterion has been most commonly used to describe the anisotropic yielding in most metals [2]. Further, the von Mises and Tresca yield criterions [3,4] for isotropic materials have been generalized and given a non-quadratic model defined in the principal stress space by Hosford in Ref. [5]. Likewise, an anisotropic extension of the Hosford model has been proposed by Hill in Ref. [6]. The yield criterions have been typically plotted as yield loci in the octahedral π-plane with deviatoric stresses along the axis. Since in sheet metal forming processes, the out-of-plane stresses are neglected, the yield loci can also be plotted in the plane-stress plane. Anisotropic yield criteria specific to sheet metals have also been developed in the principal stress space in Refs. [7–9]. Among them, the Vegter yield criterion [7,8] has been used to develop and characterize the yield loci for sheet metals in the plane-stress plane.

The measurement of anisotropic yield parameters (Lankford coefficients: R values) is typically done by uniaxial testing (tensile loading) of sheet material with varying orientations relative to the rolling direction. For planar isotropic materials the R values are obtained by bulk loading methods such as pure shear, uniaxial tensile, plane strain tensile or an equi-biaxial tensile test. Each of these experiments are combined to measure the stress points on the plane-stress plane, between which the Bezier curve has been used to describe the yield locus independent of R values, in the Vegter yield criteria [7,8,10]. Also virtual field methods (VFM) have been used in combination with digital image correlation of strain fields to obtain parameters for anisotropic yield criteria [11]. However, VFM has been applied successfully for characterizing only certain types of yield criteria mostly for uncoated sheet metals [12]. Indentation based characterization techniques have also been modelled and designed to estimate the anisotropic plastic properties [13–15] from measured results. Using the load-depth curve and the pile-up height modelled utilizing spherical indenters, the yield

* Corresponding author.
E-mail addresses: t.mishra@utwente.nl (T. Mishra), m.b.derooij@utwente.nl (M. de Rooij), m.p.shisode@utwente.nl (M. Shisode), j.hazratimarangalou@utwente.nl (J. Hazrati), d.j.schipper@utwente.nl (D.J. Schipper).

https://doi.org/10.1016/j.surfcoat.2019.125110
Received 13 September 2019; Received in revised form 23 October 2019; Accepted 26 October 2019

stress ratio has been derived for planar isotropy [14,15]. FE models involving indentation near free edge, free corner, interface of bonded samples and linear and circular scratch tests have also been used to characterize anisotropic yield parameters [13]. However, a rigorous development of a measurement and characterization method based on such indentation techniques is unavailable.

Among the pyramidal shaped indenters commonly used for hardness measurements [16], the use of an asymmetric Knoop indenter [17] with a rhombic base having diagonals of lengths in ratio 7: 1 has been used to measure the anisotropy in plastic deformation of metals. The dependence of the measured hardness on orientation of the long diagonal of the Knoop indenter relative to the crystal planes has been observed and explained using the resolved shear stress of the slip systems for hexagonal single crystal of WC, zinc and zircalloy-2 in Refs. [18–20]. However, for larger indentations over multiple grains, a flow surface theory relating the deviatoric shear stress to the indentation hardness and the geometry of the Knoop indenter was first proposed by Wheeler and Ireland [21]. By aligning the diagonals of the Knoop indenter along the principal axes of stress (axes of anisotropy), six indentations were performed on zircalloy-2 specimens. The Knoop hardness number (KHN) specific to each indentation was plotted in the octahedral (deviatoric stress) plane by taking the ratio of the corresponding deviatoric stress as equal to the ratio of the diagonal lengths of the Knoop indenter, *i.e.* 7: 1. The yield locus was plotted using the points on the plane and the strain ratios were compared with those obtained from bulk tensile tests along the anisotropic axes to good agreement.

This technique of characterizing the yield loci from KHN data of anisotropic metals was modified by relating the hardness number to plane-stress yield loci and implemented in Ref. [22] for two titanium alloys. By relating the ratio of plastic strain underneath the indenter to the ratio of its diagonal lengths and using constancy of volume of deformed substrate and the Lévy-Mises equations, the strain ratios could be related to the stress ratios in the plane-stress plane. The yield loci were plotted by equating the KHN with the equivalent stress for Hosford yield criteria [22] and compared with the yield loci obtained by tensile tests [23] at various strains to give the best agreement at 0.01 strain. The KHN-based yield loci of highly anisotropic single magnesium crystal, polycrystalline magnesium sheets and magnesium alloys in plane-stress plane were also compared with conventional yield loci for small strains in Ref. [24] but did not show good agreement. Wonsiewicz and Wilkening [24] also observed the insensitivity of the KHN-based yield loci to capture the difference in compression and in tension as well as the excessive bulk of the KHN-yield locus into plane-stress plane's quadrants for the stress ratios computed using the techniques in Ref. [22]. Hence, the R value was included in the calculation of the stress ratios from the strain ratios in Ref. [24]. Using the initial methods to plot a yield locus from KHN [21,22,24], the yield loci of pure polycrystalline titanium [25], titanium alloys [26] and zircalloys [27,28] have been determined.

Although the yield loci plotted from the indentation hardness seems convenient for bulk polycrystalline metals and alloys as has been discussed above, micro-hardness indentation of a coating along the anisotropic axes (surface and cross-section) is challenging. Hence, attempts to utilize depth-sensing Nano indentation techniques with a Knoop indenter are made in Refs. [29,30]. The hardness of the indent is measured from the maximum penetration depth in the load-depth curve or the long diagonal lengths. However, compared to the standard Berkovich tip, the elastic recovery along the shorter diagonal of the residual impression by the Knoop indenter is accounted for. In order to express the elastic modulus, the ratio of the short and the long diagonals of the residual impression by the Knoop indenter is used [30]. Knoops indentation has also been analysed by modelling the indentation response of substrate with elastic and elastoplastic material behaviour without [31] and with strain hardening effects [32]. Numerical simulation of the depth-sensing indentation tests with a Knoop indenter on substrates with various hardening and material properties were also done recently using 3D finite element models to measure the area function, hardness and the elastic modulus [33,34]. Knoop indentations have been also performed on ductile metals and brittle ceramics and the results have been compared to other pyramidal shaped indenters (Berkovich and Vickers) [35,36]. The slip anisotropy has been determined from the indentation anisotropy by Knoop nano-indentation of SiC–6H single crystals [37].

The available research to measure the yield criteria for anisotropic material has mostly focussed on bulk metals and alloys and not on surfaces and coatings. Thus far, experimental techniques to characterize the parameters for yield criteria or yield locus for coated systems have not been investigated. Moreover, zinc coatings applied on steel sheets used in deep-drawing have a high degree of anisotropy [38,39] due to orientation of the zinc grains during the prior galvanization and temper rolling processes. However, the yield criterion for zinc layer in galvanized steel sheets is unavailable in the literature. Among the available characterization techniques for coating, nano-indentation using depth sensing indentation has been mostly focussed upon [40]. Nano-indentation of zinc coating has been done to quantify the elastic anisotropy by measuring the elastic modulus and hardness for various grain orientations in Ref. [41]. Furthermore, yield loci have been plotted for various anisotropic materials using Knoop indentation [42] and have shown fair agreement with conventional yield loci.

Knoop indenter has not been used in Nano-indentation to plot obtain the yield locus of zinc coating on steel sheet so far. With the current advances in technology, modelling and analysis of Nano-indentation using the Knoop indenters, the Knoop indentation of both the surface and cross-section of zinc coating on steel substrate has been performed in the current research. A methodology to determine the parameters for Hill ’48 yield criteria [32] from Knoop hardness number is designed. The current method accounts for the anisotropic behaviour of the coating by measuring the stress ratios induced by asymmetric Knoop indenter. The yield parameters are compared with those obtained by standard tests for a cold-rolled DC04 steel sheet, thereby validating the methodology. The same method is then implemented for measuring the yield parameters for the zinc coating in the temper-rolled, galvanized steel sheets as modelled by the Hill ’48 yield criterion.

1.1. Calculation of yield parameters from KHN

A systematic procedure to derive the yield criteria for the zinc coating through indentation hardness data has been laid out in this section. Hill's quadratic yield function [2] is chosen for its ability of being expressed in matrix vector product form and hence the ease of implementation in numerical codes. Hills yield parameters have been related to the Lankford coefficients. Accounting for the anisotropy, the stress ratios in plane-stress condition have been expressed in terms of the Lankford coefficients and the strain ratio corresponding to each (six) Knoop indentation as explained in Ref. [21].

Some of the key assumptions as obtained from the literature and used in the method described below to obtain the yield parameters using Knoop indentation hardness are as follows:

1. The Knoop hardness number KHN in kgf/mm^2 is approximated to be equal to the equivalent flow stress, *i.e.* KHN is taken proportional to the shearing stress on the octahedral plane and (uniaxial) yield strength in plane stress [22,43].
2. The ratio of the deviatoric strain along the long and short diagonals of the Knoop indenter is assumed to be 1/7 [21].
3. The loading (strain) path of the Knoop indentation resulting in the intersection of the KHN based stress points with the yield locus is assumed to be linear [21,22].
4. The contact between the Knoop indenter and the experimental specimen is assumed to be frictionless and adhesionless.

1.2. Hill's yield criterion and flow rule

The quadratic Hill's yield function $f(\sigma_{ij})$ also named as the Hill 48 yield criterion [2] has been used in the current work to quantify the anisotropy in sheet metals, see equation (1.1). The Hill 48 yield criterion assumes no difference between the tensile and compressive yield stresses in a particular stress direction. The yield criterion depends on the deviatoric stresses and is pressure independent. Hence, σ_{ij} are deviatoric stresses where $i, j\varepsilon 1,2,3$ being the anisotropic axes and F, G, H, L, M and N are constants which are experimentally determined. For a rolled sheet metal, 1 is the rolling direction RD, 2 is the transverse direction TD and 3 is the normal direction ND. Typically, the constants F, G and H are determined from uniaxial yield stresses with respect to the axes of anisotropy σ_{11}^{y}, σ_{22}^{y} and σ_{33}^{y} while the constants L, M and N are determined from shear yield stresses associated to the same directions σ_{23}^{y}, σ_{31}^{y} and σ_{12}^{y} as shown in equation (1.2). The Hill's 48 yield criterion is expressed in equation (1.3) for the principal stresses σ_1, σ_2 and σ_3 aligned with the directions of anisotropy, $k\varepsilon 1,2,3$ being the principal stress axes. Further assuming associated flow for plasticity in metals, the associated flow rule is expressed in equation (1.4) using $\dot{\lambda}$ which is the rate of the plastic multiplier. The flow rule represents the coincidence between the plastic potential and the yield surface and gives the plastic deformation rate $\dot{\varepsilon}^{p}$ as orthogonal to the yield surface.

$$2f(\sigma_{ij}) \equiv F(\sigma_{22}-\sigma_{33})^2 + G(\sigma_{33}-\sigma_{11})^2 + H(\sigma_{11}-\sigma_{22})^2 + 2L\sigma_{23}^2 + 2M\sigma_{31}^2 + 2N\sigma_{12}^2 = 1 \tag{1.1}$$

$$F = \frac{1}{2}\left[\frac{1}{(\sigma_{22}^{y})^2} + \frac{1}{(\sigma_{33}^{y})^2} - \frac{1}{(\sigma_{11}^{y})^2}\right],\ G = \frac{1}{2}\left[\frac{1}{(\sigma_{33}^{y})^2} + \frac{1}{(\sigma_{11}^{y})^2} - \frac{1}{(\sigma_{22}^{y})^2}\right],$$
$$F = \frac{1}{2}\left[\frac{1}{(\sigma_{11}^{y})^2} + \frac{1}{(\sigma_{22}^{y})^2} - \frac{1}{(\sigma_{33}^{y})^2}\right],$$
$$L = \frac{1}{2(\sigma_{23}^{y})^2},\ M = \frac{1}{2(\sigma_{31}^{y})^2},\ N = \frac{1}{2(\sigma_{12}^{y})^2} \tag{1.2}$$

$$f(\sigma_k) \equiv F(\sigma_2-\sigma_3)^2 + G(\sigma_3-\sigma_1)^2 + H(\sigma_1-\sigma_2)^2 = 1 \tag{1.3}$$

$$\dot{\varepsilon}_k^{p} = \dot{\lambda}\frac{\partial f}{\partial \sigma_k} \Rightarrow \frac{\partial \varepsilon^{p}}{\partial \lambda} = \frac{\partial f}{\partial \sigma_k} \tag{1.4}$$

1.3. Relationship between yield parameters and Lankford coefficients

Typically, for thin rolled sheets, a plane-stress condition is assumed where $\sigma_3 = 0$. The yield criteria in plane-stress condition, *i.e.* for a planar anisotropic material is given in terms of principal stresses, uniaxial yield stress in rolling direction σ_1^{y} and Lankford coefficients in equation (2.1). The Lankford coefficients or the plastic strain ratios R_0, R_{90} and R_{45} are the ratios of in-plane plastic strain to out of plane (through thickness) plastic strain due to loading under uniaxial stress σ_1, σ_2 and σ_{12} (at an angle $\theta = 0^{\circ}$, 90° and 45° relative to the rolling direction) respectively as defined in equation (2.2). The relationship between the Lankford coefficients and the Hill's parameter in equation (2.2) has been derived from the flow rule in equation (1.4). The Hill's yield criterion is written for plane-stress condition in the anisotropic axes taking σ_{13}, σ_{23}, $\sigma_{33} = 0$ in equation (2.3). Hill's yield criteria in plane-stress is written in terms of the Lankford coefficients in equation (2.4) [44]. By comparing the individual terms in equations (2.3) and (2.4), the relationships between Hill's yield parameters and the Lankford coefficients are obtained in equation (2.5). For planar isotropy, the plastic strain ratio R_0 is independent of θ and $R_{90} = R_{45} = 1$. By substituting values of the yield parameters F, G and H in equation (1.4), the equivalent flow stress is expressed in the principal stresses as given in equation (2.6).

$$f(\sigma_k) = \sigma_1^2 - \frac{2R_0}{R_0+1}\sigma_1\sigma_2 + \frac{R_0(R_{90}+1)}{R_{90}(R_0+1)}\sigma_2^2 = (\sigma_y)^2\ \forall\ \sigma_3 = 0 \tag{2.1}$$

$$R_0 = \frac{d\varepsilon_2}{d\varepsilon_3} = \frac{H}{G}\ \forall\ (\theta = 0);\ R_{90} = \frac{d\varepsilon_1}{d\varepsilon_3} = \frac{H}{F}\ \forall\left(\theta = \frac{\pi}{2}\right);\ R_{45} = \frac{d\varepsilon_{12}}{d\varepsilon_3} = \frac{H}{F+G} - \frac{1}{2}\ \forall\left(\theta = \pm\frac{\pi}{4}\right) \tag{2.2}$$

$$2f(\sigma_{ij}) = (G+H)\sigma_{11}^2 - 2H\sigma_{11}\sigma_{22} + (F+H)\sigma_{22}^2 + 2N\sigma_{12}^2 = 1\ \forall\ \sigma_{13},\ \sigma_{23},\ \sigma_{33} = 0 \tag{2.3}$$

$$f(\sigma_{ij}) = \sigma_{11}^2 - \frac{2R_0}{R_0+1}\sigma_{11}\sigma_{22} + \frac{R_0(R_{90}+1)}{R_{90}(R_0+1)}\sigma_{22}^2 + \frac{(R_0+R_{90})(2R_{45}+1)}{R_{90}(R_0+1)}\sigma_{12}^2 = 1 \tag{2.4}$$

$$F = \frac{R_0}{R_{90}(R_0+1)},\ G = \frac{1}{R_0+1},\ H = \frac{R_0}{R_0+1},\ N = \frac{(R_0+R_{90})}{R_{90}(R_0+1)}\left(R_{45}+\frac{1}{2}\right),\ M = \frac{3}{2},\ L = \frac{3}{2} \tag{2.5}$$

$$\sigma_f^2 = \frac{R_0(\sigma_1-\sigma_2)^2 + R_0R_{90}(\sigma_2-\sigma_3)^2 + R_{90}(\sigma_3-\sigma_1)^2}{R_0R_{90}+R_{90}} \tag{2.6}$$

1.4. Derivation of stress ratio's using anisotropy constants

The ratio of plastic strain underneath the Knoop indenter along the long and short diagonal is assumed proportional to the inverse of the ratio of the length of the diagonals, *i.e.* $d\varepsilon_{D_l}^{p}/d\varepsilon_{d_s}^{p} = d_s/D_l = 1/7$ as shown in Fig. 1a. This results from the plastic deformation (displacement of substrate) along the diagonals of a penetrating Knoop indenter follows the projected length the edges of the faces of the indenter in contact with the substrate. Following the work done in Ref. [21], the diagonals of the Knoop indenters are oriented along the principal coordinate direction which are also aligned along the axes of anisotropy (RD, TD and ND). In the analysis, the axes of anisotropy for the measured specimen

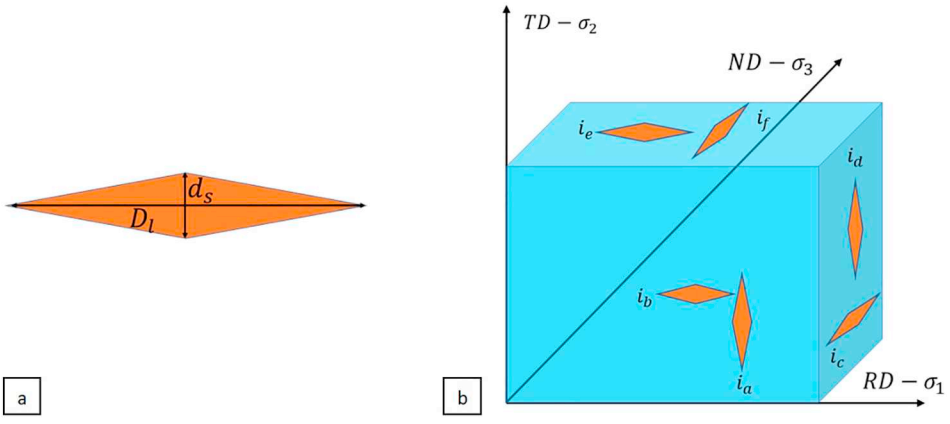

Fig. 1. (a) The geometry of a Knoop indent showing lengths of short diagonal d_s and long diagonal D_l and (b) the orientation of six Knoop indentations i_a, i_b, i_c, i_d, i_e and i_f with D_l and d_s along RD (Rolling direction), TD (Transverse direction) and ND (Normal direction).

are supposed to be known in advance. So, the sides of the Knoop indenter can be aligned with the anisotropy direction. This is the case for six possible indentations namely i_a, i_b, i_c, i_d, i_e and i_f as shown in Fig. 1b. In plane-stress condition the yield criterion is expressed in terms of principal stresses σ_1 and σ_2. Hence the strain ratios of the indentations i_a and i_b corresponding to the $\sigma_1 - \sigma_2$ plane are taken as 1/7 and 7. The other strain ratios corresponding to the indentations i_c, i_d, i_e and i_f are obtained from volume constancy, *i.e.* $d\varepsilon_1^p + d\varepsilon_2^p + d\varepsilon_3^p = 0$. The strain ratios on the $\sigma_1 - \sigma_2$ plane are given in equation (3.1) as a vector $\boldsymbol{B}$ using the ratio $\delta = 7$. By using the associated flow rule the expression for the strain ratio vector $\boldsymbol{B}$ has been expanded in equation (3.2) following which the stress ratio vector, *i.e.* the ratio of principal stresses in plane stress-plane $\alpha = \sigma_2/\sigma_1$ for each indentation ($i_a - i_f$) has been expressed in terms of Lankford coefficients, and strain ratio vector $\boldsymbol{B}$. The expression of α in equation (3.3) accounts for the anisotropy in the specimen characterized for its yield criterion parameters.

$$\boldsymbol{B} = \frac{d\varepsilon_2}{d\varepsilon_1} = [\, B_a \;\; B_b \;\; B_c \;\; B_d \;\; B_e \;\; B_f \,] = \left[\frac{1}{\delta} \;\; \delta \;\; -\frac{\delta}{1+\delta} \;\; -\frac{1}{1+\delta} \;\; -\delta - 1 \;\; -\frac{1+\delta}{\delta} \right] \tag{3.1}$$

$$B = \frac{d\varepsilon_2}{d\varepsilon_1} = \frac{\frac{\partial f}{\partial \sigma_2}}{\frac{\partial f}{\partial \sigma_1}} = \frac{\frac{2R_0(R_{90}+1)}{R_{90}(R_0+1)}\sigma_2 - \frac{2R_0}{R_0+1}\sigma_1}{2\sigma_1 - \frac{2R_0}{R_0+1}\sigma_2} \tag{3.2}$$

$$\Rightarrow \alpha = \frac{\sigma_1}{\sigma_2} = \frac{R_0}{R_{90}} \frac{\boldsymbol{B}R_{90} + R_{90} + 1}{\boldsymbol{B}R_0 + \boldsymbol{B} + R_0} \tag{3.3}$$

1.5. Plotting points on $\sigma_1 - \sigma_2$ plane from KHN data

The Knoop hardness number is taken proportional to the deviatoric shearing stress on the octahedral plane. Therefore, the KHN is assumed to be equivalent to the equivalent flow stress (uniaxial yield stress) in plane stress as explained in Ref. [22] and is in agreement with [43]. For the Hill's 48 yield criterion the equivalent stress in plane stress condition is given as the uniaxial yield stress in the (rolling direction) principal axis 1, σ_1^y. By equating the Knoop hardness number with uniaxial yield stress ($KHN \sim \sigma_1^y$), equation (4.1) can be obtained. By expressing equation (4.1) in terms of ratios of σ_1 and σ_2, *i.e.* α for each indentation i_a, i_b, i_c, i_d, i_e and i_f the expressions for the points (coordinates) on the KHN yield locus are obtained in the $\sigma_1 - \sigma_2$ plane as given in equation (4.2).

$$KHN \sim \sqrt{\sigma_1^2 - \frac{2R_0}{R_0+1}\sigma_1\sigma_2 + \frac{R_0(R_{90}+1)}{R_{90}(R_0+1)}\sigma_2^2} \tag{4.1}$$

$$\sigma_1 \sim \frac{\alpha_i KHN_i}{\sqrt{(C_1 - C_2\alpha_i + \alpha_i^2)}}, \qquad \forall\, C_1 = \frac{R_0(R_{90}+1)}{R_{90}(R_0+1)}$$

$$\sigma_2 \sim \pm \frac{KHN_i}{\sqrt{(C_1 - C_2\alpha_i + \alpha_i^2)}} \;\; \forall\; i \varepsilon i_a, i_b, i_c, i_d, i_e \qquad , C_2 = \frac{2R_0}{R_0+1} = 2C_0$$

$$, i_f \tag{4.2}$$

The Knoop hardness number (KHN) is measured using the dimensions of the indentation mark as shown in Fig. 1a. The KHN is given as the ratio of the applied load P and the area of the indentation A_c. The area of the indent is given is terms of the major diagonal length D_l of the indentation mark and a constant factor $C_K = 0.070279$. For the Knoop indenter, the contact area is given in terms of the indentation depth h as $A = 64.55h^2$. Using the relationship between the indentation depth h and major diagonal length as $D = 30.514h$, KHN is given in terms of h in equation (5.1) in Kgf/mm^2 units and in terms of h and D in equation (5.2) in GPa units [29]. The Young's modulus E of the specimen is calculated from the elastic recovery of the indented material during unloading of the indenter [45]. However, the elastic recovery along the shorter diagonal of the Knoop indenter is higher compared to that of the longer diagonal of the Knoop indenter [30]. The difference in the recovered (final) contact length ratio and the maximum contact length (7.114) is proportional to the ratio $KHN\,[GPa]/E$. Hence, the Young's modulus of the specimen can be calculated by equation (5.3) using a geometry factor of 0.45 [30,51].

$$KHN = \frac{P}{A_c} \Rightarrow KHN = 14.229\frac{P\,[Kgf]}{D_l^2\,[mm^2]} \tag{5.1}$$

$$\Rightarrow KHN\,[GPa] = 0.13944\frac{P\,[N]}{D_l^2\,[mm^2]} = 0.015492\frac{P\,[mN]}{h^2\,[\mu m^2]} \tag{5.2}$$

$$\frac{d_s}{D_l} = \frac{1}{7.114} - 0.45\frac{KHN}{E} \tag{5.3}$$

1.6. Optimizing the yield parameters based on KHN-data points

The yield parameters R_0, R_{90} and σ_y obtained for the yield locus fitting the KHN based points for all six orientations plotted in the $\sigma_1 - \sigma_2$ plane (equation (4.2)) is optimized by minimizing the distance between the yield locus and the KHN based points in the $\sigma_1 - \sigma_2$ plane. The distance between the KHN data points (σ_1, σ_2) and the yield locus is measured along a straight line using either of the two methods described below. In both the methods, a linear strain path is assumed for the Knoop indentation to find the intersection of the KHN data points with yield locus as shown in Fig. 2.

The distance between the points plotted using equation (4.2) from the KHN-data (σ_1, σ_2) and the yield locus plotted from R_0 and R_{90} values obtained by solving the equation for the ellipse in the $\sigma_1 - \sigma_2$ plane for the plotted KHN-data points is calculated by two methods. In the first method the shortest distance between the points and the yield locus is calculated taking the perpendicular line from the points and the intersection with the yield locus. The slope of the perpendicular line to the ellipse is given as m_n and the slope of the ellipse (yield locus) at the point of intersection is given as m_e as shown in Fig. 2. In the second method, the distance between the KHN points and the yield locus along the line through the origin and the KHN points intersecting the yield locus is minimized. The slope of the line passing through the origin of the plane-stress plane and the measured points using KHN data points is given as m_s as shown in Fig. 2. The point of intersection (σ_1', σ_2') for the normal to the yield locus, passing through the KHN-data point is given by solving equations (6.1) and (6.2). The point of intersection (σ_1', σ_2') along the line from the origin to the KHN-data points by solving equations (6.2) and (6.3). The total distance $\boldsymbol{d}$ between the KHN-data points and the intersecting points on the yield locus is given as the norm of distance between the individual KHN points d_i (σ_1, σ_2) and the points of intersection (σ_1', σ_2').

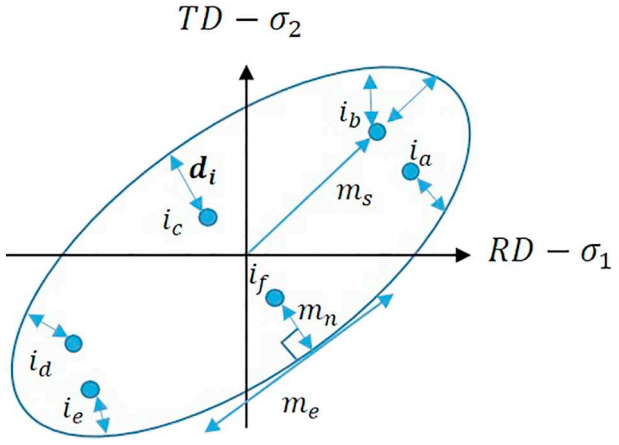

Fig. 2. Minimization of distance between the points plotted in the plane-stress plane and the yield locus obtained from the values of R_0, R_{90} and σ_y.

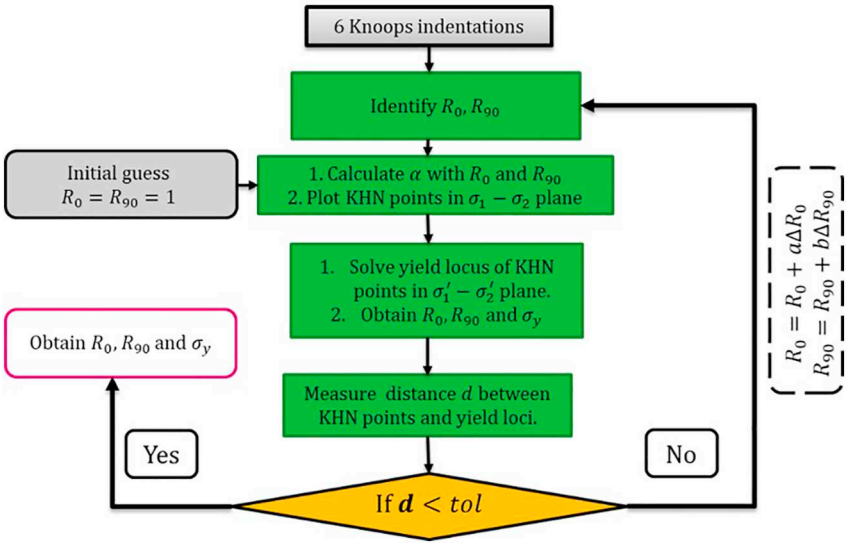

Fig. 3. Flowchart showing the optimization algorithm to obtain values of R_0, R_{90} and σ_y.

$$m_n m_e = -1 \;\; \forall \; m_n = \frac{\sigma_2' - \sigma_2}{\sigma_1' - \sigma_1},$$

$$m_e = \frac{d\sigma_2'}{d\sigma_1'} = -\frac{\frac{\partial f}{\partial \sigma_1'}}{\frac{\partial f}{\partial \sigma_2'}} = -\frac{2\sigma_1' - \frac{2R}{R+1}\sigma_2'}{\frac{2R(P+1)}{P(R+1)}\sigma_2' - \frac{2R}{R+1}\sigma_1'} = -\frac{\sigma_1' - C_0\sigma_2'}{C_1\sigma_2' - C_0\sigma_1'}$$

$$\Rightarrow C_1(\sigma_1'^{\,2} - \sigma_2'^{\,2}) + (1 - C_1)\sigma_1'\sigma_2' + (C_1\sigma_2'\sigma_1 - \sigma_1'\sigma_2) + C_0 (\sigma_2'\sigma_2 - \sigma_1'\sigma_1) = 0 \tag{6.1}$$

$$\sigma_1'^{\,2} - 2C_0\sigma_1'\sigma_2' + C_1\sigma_2'^{\,2} - \sigma_1^{y\,2} = 0 \tag{6.2}$$

$$m_s = \frac{\sigma_2}{\sigma_1} = \frac{\sigma_2'}{\sigma_1'} \Rightarrow \sigma_2' = m_s\sigma_1' \tag{6.3}$$

$$d_i = \sqrt{(\sigma_1' - \sigma_1)^2 + (\sigma_2' - \sigma_2)^2} \Rightarrow \boldsymbol{d} = d_i = \sqrt{\sum_{i=1}^{6} d_i^2} \tag{6.4}$$

The values of R_0, R_{90} and σ_y are chosen and changed such that the distance between the KHN-data points and the yield locus is minimized in the $\sigma_1 - \sigma_2$ plane as shown in Fig. 2. The optimization function selects various values of R_0, R_{90} and σ_y using an objective function where distance d is minimized as further explained in Fig. 2. The KHN data for all 6 orientations are used to measure the coordinates in the $\sigma_1 - \sigma_2$ plane by taking an initial values of $R_0 = 1$ and $R_{90} = 1$. The initial value of R_0 and R_{90} are varied across a range of values until the distance between the points and the yield locus is minimized.

To further analyse the data, an algorithm to plot the yield locus from the KHN data and to calculate R_0, R_{90} and σ_y has been developed and shown in Fig. 3. Initially, points are plotted in the deviatoric plane from KHN, using equation (3.1) ($\alpha = \boldsymbol{B}$) and 3.3 ($R_0 = R_{90} = 1$) respectively. However, the yield locus obtained in the deviatoric plane or for that matter in the plane-stress plane with an isotropic assumption of $R_0 = R_{90} = 1$ is not accurate for anisotropic material. Also, typically sheet metal processes have used plane stress assumptions in expressing anisotropic material behaviour. Hence, an algorithm has been developed to optimize the value of R_0 and R_{90} and use the optimized values to plot the yield locus in the plane-stress plane. The algorithm minimizes the distance between the points plotted in the plane-stress plane using KHN-data. Then, the yield locus plotted in the plane stress plane using the optimized values of R_0, R_{90} and the value of σ_y.

2. Experimental procedure

Anton Paar's NHT^3 nano-indentation set-up along with the Knoop indenter is used to perform nano-indentation of both zinc coated and uncoated steel sheets. For higher loads Lecco's LM100 micro hardness test set up was used with a Knoop indenter. The geometry of the Knoop indenter is explained in the current section. Also metallographic preparation of steel sheets has been done prior to the indentation as explained in this section. The polished sheets are also used for EBSD (electron backscatter diffraction) analysis in SEM (scanning electron microscopy) to study the grain size and grain orientation in the sheets. The surface of the specimen is measured using a confocal microscope for its roughness after polishing.

2.1. Preparation of specimens

Knoop indentation based characterization has been done on low carbon DC04 steel sheets and zinc coating on steel sheets. Prior to characterization polishing of the sheets is done which serves a two-fold purpose. The effect of friction on the maximum resolved deviatoric stress on the surface of the Knoop indenter is minimized by polishing. The aim is to equate the Knoop hardness to the deviatoric stress resulting in plastic flow of the sheet due to indentation. By comparing the size of the indent with the grain size the indentation loads are adjusted such that the indentation measurements are done for multiple grains.

Both the DC04 steel sheet and the zinc coated steel sheets have been obtained from cold rolling mills with a marked rolling direction. They have been cut into rectangular sheets of different sizes for polishing of the surface and the cross-section. Rectangular sheets of length 10 *mm* and with 15 *mm* with the rolling direction along the length have been laser cut from the rolled sheets and used for polishing the surface. The cross section of rectangular sheets of length 10 *mm* cut along transverse direction of length 15 mm cut along rolling direction and width 2.5 mm width have been polished as well. The surface of the 10 × 15 mm sheets and the cross-section of the 10 × 2.5 mm and 15 × 2.5 mm are hot mounted using a bakelite disc of 25 mm diameter for the metallographic preparation.

An automatic polishing machine was used to polish the mounted bakelite discs. The following polishing steps are used for the surface and cross-section of the DC04 steel sheets. Grinding of the steel sheets is done initially using 220 grade silicon carbide paper at 25 N load and 300 rpm for 3 min using water as lubricant. Further grinding was done using diamond suspension of 9 µm particle size at 40 N load and 150 rpm for 5 min. The grinding steps removed unevenness on the surface of the steel sheet. Further polishing was done in three steps. Diamond suspensions with 3 µm and 1 µm particle sizes were used at 20 N load 150 rpm for 4 min. For the final etching step, a silica

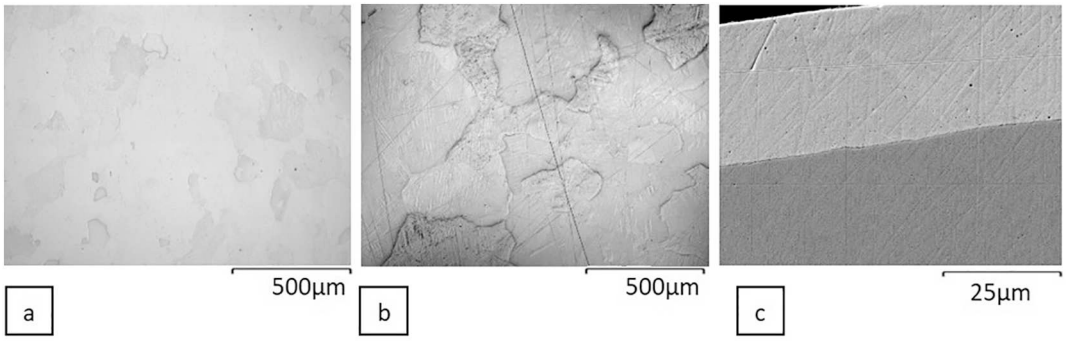

Fig. 4. Surface of the polished and etched (a) DC04 steel sheet and (b) zinc coating on steel sheet at 20x magnification seen using confocal microscopy and (c) cross-section of the zinc coated steel sheet at 1900x magnification seen using SEM.

suspension of 0.04 µm was used at 15 N load 150 rpm for 3 min. This results in a surface roughness of 20 nm on the steel surface as shown in Fig. 4a.

The polishing of the zinc coating using similar steps is challenging due to the softness of the coating, the shrinkage gap between the coating and the bakelite resin mount and the reaction of water with the coating resulting in discoloration. Hence water and water based lubricants are only used in the initial grinding of the zinc coating cross-section using 320 grade sandpaper at 300 rpm and 9 µm particle size diamond suspension at 150 rpm both at 30N load for 4 min respectively. To avoid the reaction of water, an alcohol based lubricant with diamond slurries of 3 µm and 1 µm are applied at 25 N and 20 N at 150 rpm for 4–6 min respectively. The final etching of the zinc coating was done using de-agglomerated gamma alumina powder of 0.05 µm mixed with Ethanol denatured with iso-propyl alcohol at 15 N and 150 rpm for 2 min. In order to polish the surface of the zinc coating on the steel sheet without removing the soft zinc coating, the grinding steps are avoided and only polishing and etching steps are followed similar to that of the zinc coating cross-section. The polished surface and cross-section of the zinc coating is shown in Fig. 4b and c respectively. The size and thickness of the zinc grains can be estimated to be around 100–200 μm and 10–20 μm from Fig. 4b and c respectively. The slip deformation marks due to rolling process can be seen on the zinc grains in Fig. 4b.

2.2. Indentation test set-up

Anton Paar's NHT^3 nano-indentation set up has been used to perform indentation based characterization of the DC04 and zinc coated specimen as shown in Fig. 5a. Nano indentation is a depth sensing indentation technique where the applied load and the penetration depth of the indenter into the specimen are recorded and used to determine the mechanical properties of the test specimen [46]. The force is applied during indentation by a piezo-electric actuator with a feedback control. In the current work, the Nano-indentation tester can apply a load up to a maximum force of 500 mN at a resolution of 0.02 µN and a maximum penetration depth of 200 µm at a resolution of 0.01 nm. The Nano-indentation tester used, has a noise floor value of ± 0.5 μN for load controlled indentation which indicates the maximum resolution by which noise is precisely measured [47]. The schematic of the Nano-indentation test set-up and the Knoop indenter tip is shown in Fig. 5a and b.

In a depth sensing nano-indentation technique [45] the hardness and the elastic modulus of the specimen are measured using the loading and unloading curves respectively as shown in Fig. 6b. During loading the load is increased to the set load P_m for a time duration of 30 s. At maximum load P_m the load is kept constant for a dwell time duration of 10 s to avoid creep effects. The unloading is done at a similar rate as loading for a duration of 30 s. The loading and unloading sequence and the corresponding penetration depth is plotted in Fig. 6a. The hardness of the specimen H_i is measured from the ratio of the applied load to the indentation area A_c which corresponds to the maximum penetration depth h_m as given in equation (7.1) for Knoop indenter. The unloading of the indenter is followed by elastic recovery of the substrate. The stiffness of the substrate system can be given as the slope of the unloading curve in Fig. 6b. The residual elastic modulus of the indenter substrate system E_r is calculated by equation (7.2). The elastic modulus of the substrate E_s is calculated from equation (7.3), given the elastic

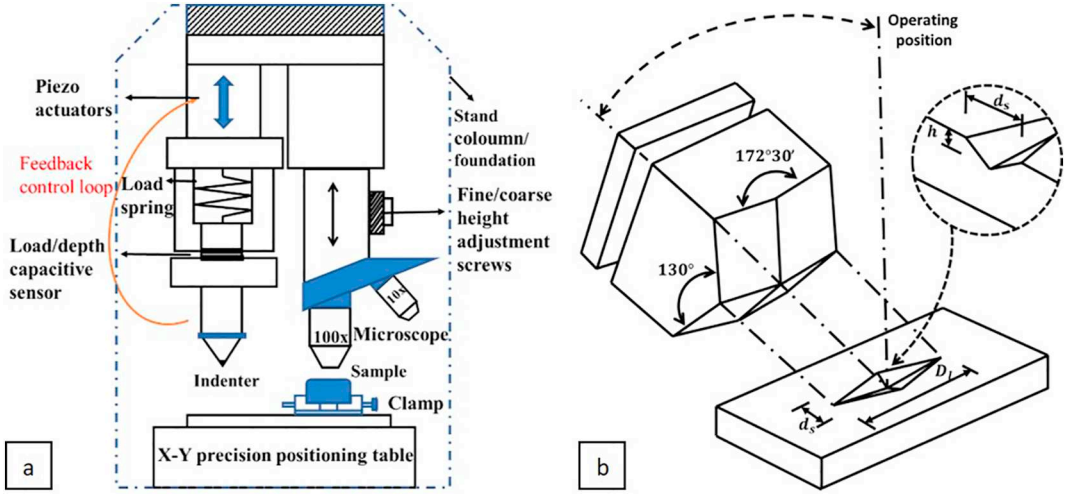

Fig. 5. Schematic of the (a) the nano-indenter set up, (b) the Knoop indenter and the indent.

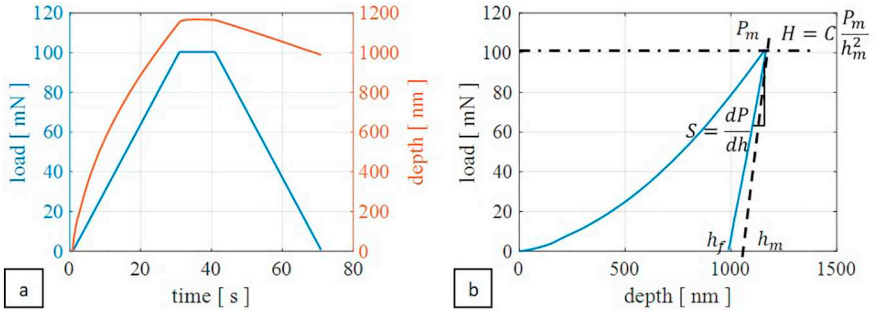

Fig. 6. (a) Loading and penetration curves for Nano-indentation using Knoop indentation (b) to obtain hardness and stiffness from the load-depth curve [46].

modulus value of the indenter E_i.

$$H_i = \frac{P_m}{A_c} \forall\, A_c = 65.44 h_m^2 \tag{7.1}$$

$$E_r = \frac{\sqrt{\pi}}{2}\frac{S}{A} \forall\, S = \frac{dP}{dh} \tag{7.2}$$

$$\frac{1}{E_r} = \frac{1-\nu_i^2}{E_i} + \frac{1-\nu_s^2}{E_s} \tag{7.3}$$

2.3. Calibration of indenter shape function

The schematic of an indent on the cross section of a coating is given in Fig. 7a. The applied load is maintained such that the size of the indent is less than the coating thickness (20 μm). However, prior to indentation experiments the tip of the Knoop indenter must be calibrated for its tip shape by a shape function. The shape function of the indenter gives the projected area of the indentation at the contact depth h_c and is approximated by fitting polynomial function to the experimentally calibrated data. The shape function takes into account the curvature of the indenter tip in measurement of the projected contact area. By indenting the calibrated fused silica specimen and curve-fitting the experimental data as shown in Fig. 7b, the shape function of the Knoop indenter in nano-indentation was obtained with equation (8) and implemented in the calibration file of the nano-indenter for Knoop indentation.

$$A_c = 97.77 h_c^2 + 5.57 \times 10^{-6} h_c + 5 \times 10^{-14} \tag{8}$$

For very large loads in micro-hardness measurement methods, where the elastic recovery is negligible compared to the indent size, the hardness can be measured by the final indent size after indentation. However, the KHN is measured with the depth sensing method at loads of 10–100 mN by equation (7.1).

3. Results and discussion

The grain size and orientations of the DC04 steel sheet and zinc coated steel sheet have been studied using SEM with EBSD analysis. Based on the grain size, the loads and distribution of in the Knoop indentations has been varied such that the anisotropy at the crystal scale is minimized. The grain orientations are also helpful in understanding the slip systems and the anisotropy in the grains with respect to rolling process.

The Knoop hardness number is measured for all 6 orientations for both the DC04 steel sheet and the zinc coating on the steel sheet. The six orientation namely i_a, i_b, i_c, i_d, i_e and i_f correspond to the orientation of the longer diagonal D_l and the shorter diagonal d_s along the anisotropy axes rolling direction RD, transverse direction TD and normal direction ND. Hence a given orientation, for instance can be written as $ND - rd$ where the long diagonal D_l is oriented along the normal direction ND and the shorter diagonal d_s is oriented along the rolling direction rd (RD). The results are plotted in the plane-stress plane. The distance between the plotted points and the yield locus $\boldsymbol{d}$ is minimized along the slope m_s. Then the anisotropy parameters are optimized using the algorithm in section 2.5 and used to plot the yield locus in plane stress plane. The KHN-based yield curve and anisotropic parameters have been validated with the yield curve and anisotropic parameters obtained using bulk tests.

3.1. Grain size and orientation of DC04 steel and zinc coating

The cross section of the zinc coated steel substrate and surface of the zinc coating showing the individual grains is given in Fig. 8. The average grain size of the zinc coating can be estimated to be around 100–200 μm. It can be seen that the zinc grains are aligned as pancakes with a thickness of 20 μm. It can be deduced from Fig. 8a and b that the size of the grains is typically in the order of the size of the Knoop indent (see Fig. 7a). If the grain size is larger than the indentation size, then the grain size and orientation has a major effect on the properties obtained from the indentation [41]. Hence larger loads are chosen for

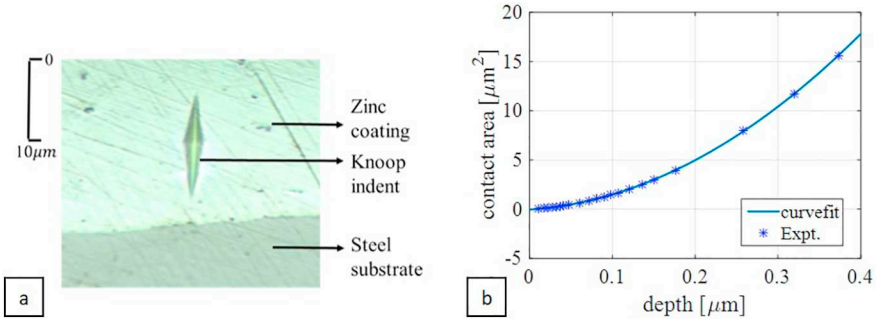

Fig. 7. (a) Schematic of Knoop indent in the coated cross-section. (b)Fitting of the contact areas obtained for various penetration depths in calibration of shape function of the tip of the Knoop indenter.

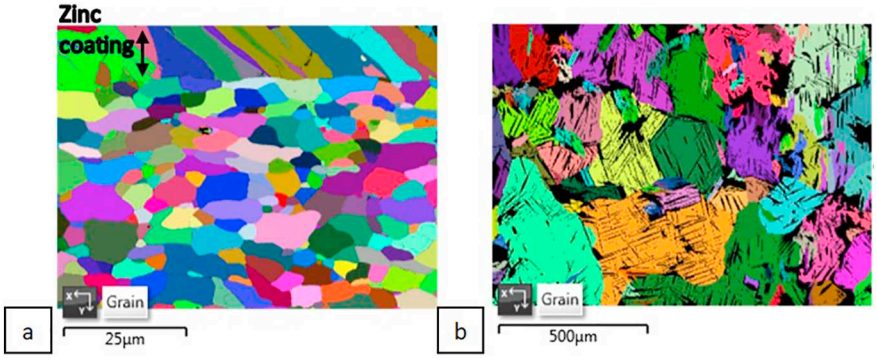

Fig. 8. Image of the grains in the (a) cross section of the zinc coating and (b) surface of the zinc coating on steel sheet after polishing and etching as seen in the backscattered image in EBSD analysis.

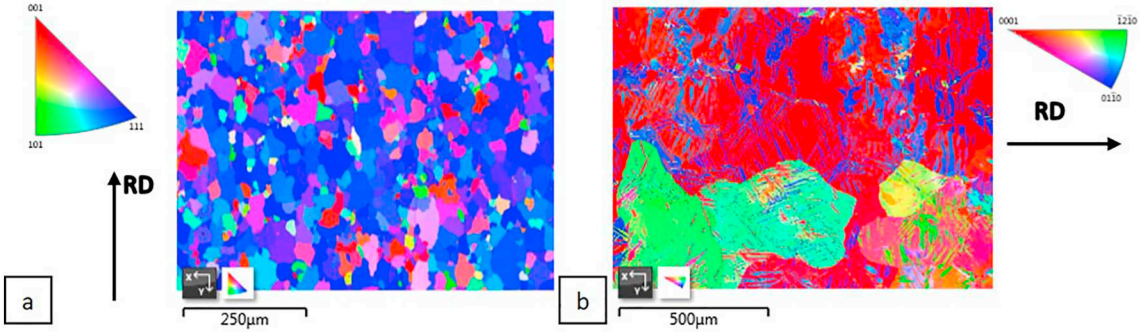

Fig. 9. Image of the inverse pole figures (IPF Z) of the grains in the surface of the (a) DC04 steel sheet and the (b) zinc coating on steel sheet after polishing and etching as seen in the EBSD analysis.

Nano-indentation keeping in mind the coating thickness for zinc coated specimens. Furthermore, multiple indentations (20–50 in number) have been performed as a matrix spread out over a region of the specimen and the average of the data obtained from the indentation is taken. This helps in averaging the effect of local grain orientation and size on the data obtained from the Knoop indentation.

Fig. 9b shows the Euler angles in the inverse pole figure (IPF Z) map of the SEM scan of the area shown in Fig. 8b. The zinc grains are mostly oriented along their (*hcp* crystals) *c* axis almost normal to the sheet plane. However certain grains can be seen elongated and aligned along the rolling direction in Fig. 9b. Multiple pyramidal slips and twins can be seen throughout the grain matrix as well. The deformation of the zinc grains during the (temper/cold) rolling process orients the zinc grains in a preferred direction as can be seen in Fig. 8a and IPF figure in Fig. 9b. The grain size of the steel substrate and the DC04 steel is much smaller around 10–20 μm from Figs. 8a and 9a. The DC04 steel grains (*bcc* (body centred cubic) crystals) are predominantly aligned with their axis along the 111 direction.

3.2. Yield locus of DC04 steel

The hardness of the DC04 steel sheet specimen was measured for each of the six orientations using 20 measurements. The average values of the Knoop hardness numbers for each six indentations were plotted for 50 g load in Fig. 10a. A maximum load of 50 g equivalent to 490.05 mN was applied using a Knoop indenter to avoid any grain effects on yield behaviour of the DC04 steel. Multiple indentations have been done, in an indentation matrix shown in Fig. 10b. The size of the Knoop indentation has been measured by observing them under a confocal microscope. The length of the long diagonal D_l, short diagonal d_s and indentation depth h of the Knoop indent mark is measured from the height profile of the indent as shown in Fig. 10c. The symbols in the bar plots below represent the orientation of the longer and shorter diagonals of the Knoop indenter along the axis of anisotropy, *e.g.* the $ND - rd$ represents the long diagonal D_l along the normal direction ND and short diagonal d_s along the rolling direction rd.

The yield locus of the DC04 steel sheet is initially plotted in the deviatoric plane as shown in Fig. 11. By assuming the Levy's Mises criteria for isotropic materials, the stress ratio is taken equal to the strain ratios from equation (3.1) ($\alpha = \boldsymbol{B}$). The six points i_a, i_b, i_c, i_d, i_e and i_f corresponding to six indentation orientations are scaled according to the Knoop hardness number given in Table 1. However, the anisotropic parameters obtained from the deviatoric yield locus are typically the same as those obtained from bulk tests for DC04 steel sheet [48]. Hence, the yield locus is plotted in the plane-stress plane and optimized to obtain the anisotropic parameters.

The initial KHN-data points are plotted in the plane-stress plane by taking initial values of $R_0 = R_{90} = 1$. The yield locus is solved for the plotted points from which values of R_0, R_{90} and σ_y are obtained. The values of R_0 and R_{90} are used to correct and re-plot the yield locus until the difference in the distance between iterated KHN-data points and the yield loci from the values of modified R_0, R_{90} and σ_y is below a specified tolerance. The optimized KHN-yield locus is plotted in the plane-stress plane in Fig. 12 and its optimized R_0, R_{90} and σ_y are listed in Table 1 and compared with those obtained from the bulk loading tests of DC04 steel [48]. The close agreement in both the methods, sets the possibility of using Knoop (Nano-) indentation with the developed algorithm given in Fig. 12 to characterize the yield locus for thin, zinc coatings of galvanized steel sheets [41].

3.3. Yield locus of zinc coating

Multiple indentations have also been performed on the cross-sections of the zinc coating as shown in the Fig. 13b and c. The size of the indents for indentation along the cross-section of coating at higher loads (> 50 *mN*) exceeds the thickness of the coating cross-section.

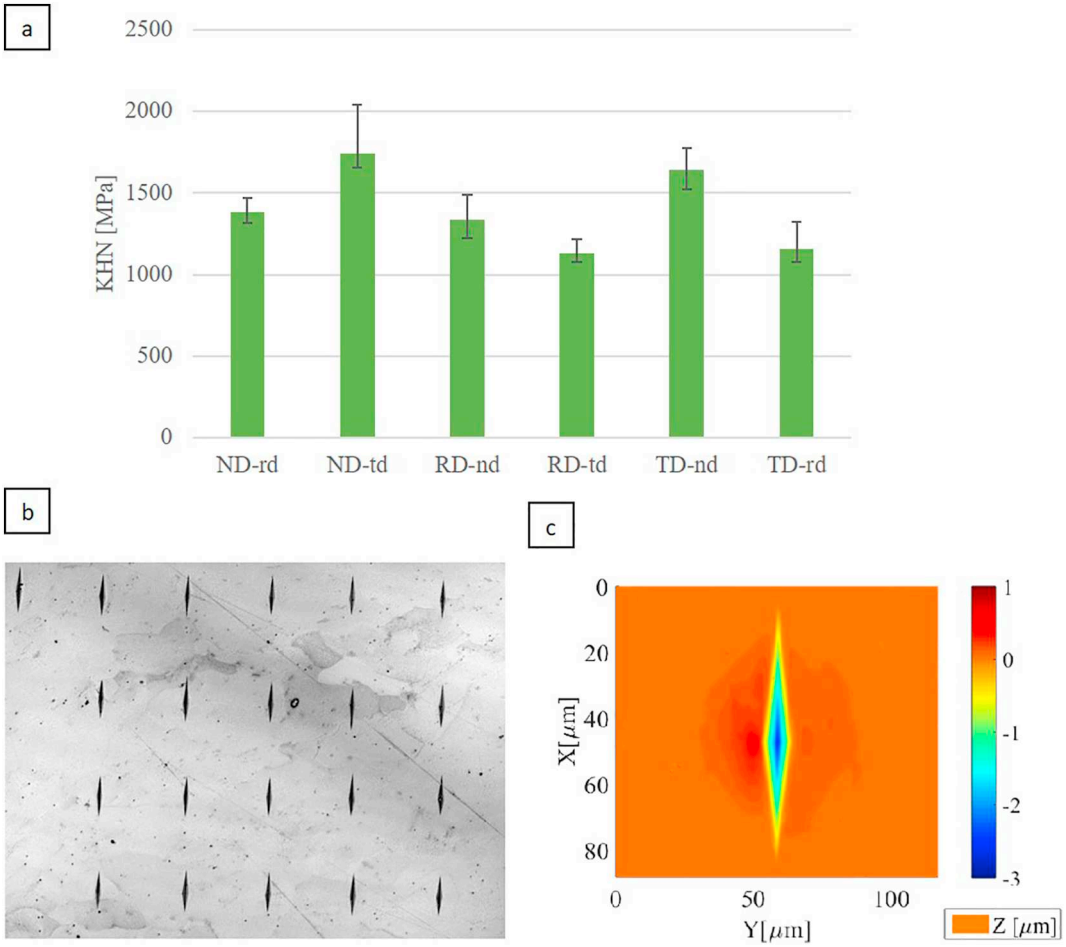

Fig. 10. (a) Mean Knoop hardness number for indentations with six different orientations on DC04 steel sheet at (50 g) 491 mN load. (b) Image of matrix of Knoop indents and (c) the height profile and size of the Knoop indent at (50 g) 491 mN load.

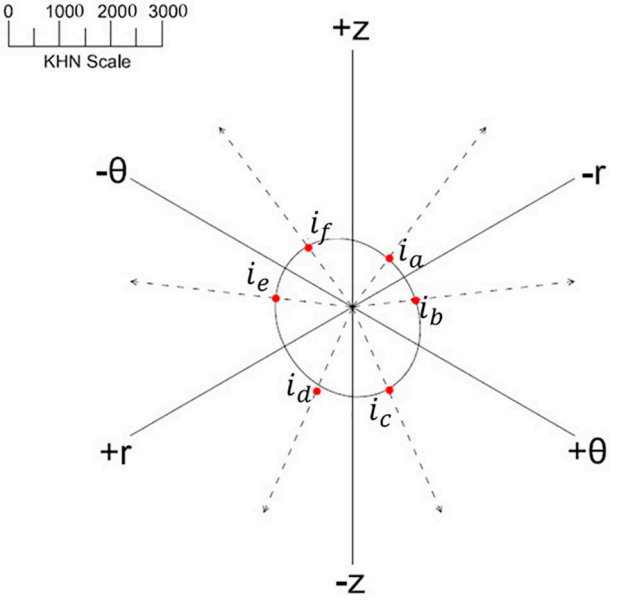

Fig. 11. Yield locus for DC04 steel sheet in the deviatoric plane in the rolling direction z, transverse direction θ and normal direction r with KHN scale in MPa.

Table 1
Knoop hardness number and Yield criteria parameters for DC04 steel sheet [48].

KHN-orientation	Value[kgf/mm^2]	Yield criteria parameters	Value
KHN_{i_a}	118.25	R_0^{bulk}	1.93
KHN_{i_b}	115.1	R_{90}^{bulk}	2.21
KHN_{i_c}	177.35	σ_y^{bulk}	157.8 MPa
KHN_{i_d}	167.4	R_0^{KHN}	1.8
KHN_{i_e}	136.55	R_{90}^{KHN}	2.34
KHN_{i_f}	141.35	σ_y^{KHN}	168.5 MPa

Hence, the indentation load is taken as 20 mN in order to keep the indentation size well within the coating thickness of 20 μm as shown in Fig. 13b. The length of the longer diagonal for the 20 mN load can be seen as 10–12 μm in Fig. 13c which is lower than the average coating thickness of 20 μm. This corresponds to a penetration depth of $h = D_l/30$ which is approximately 0.4 μm. For such low penetration depth, the plastic flow along the coating thickness direction which is also along the longer diagonal is minimal. The plastic flow occurs along the short diagonal which is along the coating. Therefore, it can be concluded that for indentations with 20 mN loads along the coating cross section, the effect of substrate mechanical properties is minimal. Furthermore, the plastic flow component under the indenter along the

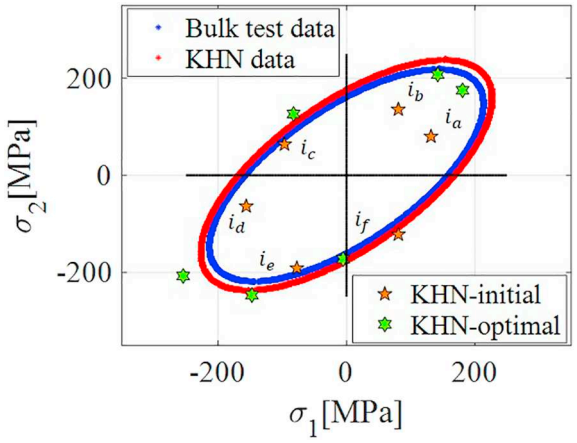

Fig. 12. The yield loci obtained from KHN data on the plane-stress plane optimized for anisotropy and compared with that obtained with bulk tests on DC04 steel sheet.

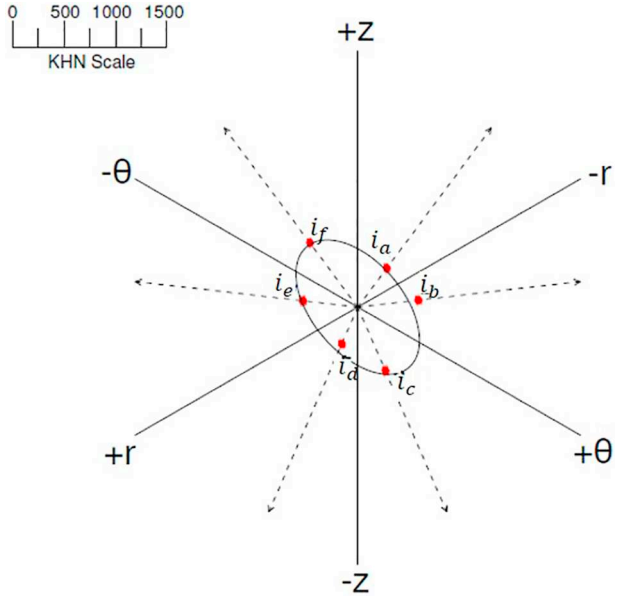

Fig. 14. Yield locus for zinc coating in the deviatoric plane in the rolling direction z, transverse direction θ and normal direction r with KHN scale in MPa.

penetration direction does not feel substrate effect for indentation along the coating cross section.

The value of Knoop hardness value for all six orientations is plotted for three different loads in Fig. 13a. A large deviation in the hardness values is obtained for each of the six indentation orientation resulting from the effect of the orientation of the zinc grains on indentation hardness (see Fig. 13a). The average value of the measurements of the indents at the same orientation are taken to reduce the local effects of anisotropy due to grain size and orientation. The average of the hardness values (KHN) obtained from indents with an applied load of 20 mN load is used to calculate the yield locus of the zinc coating in order to avoid effects of coating-substrate interface and, properties of the steel

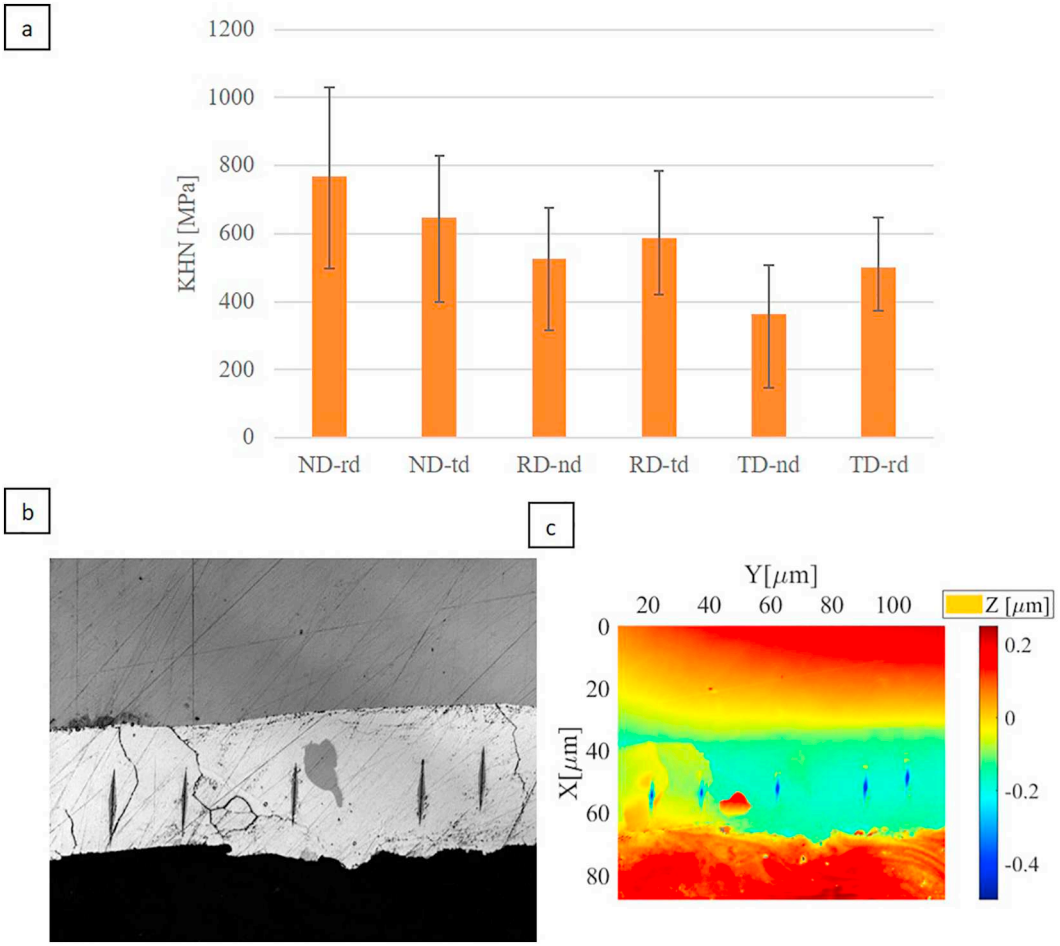

Fig. 13. (a) Mean Knoop hardness number for indentations with six different orientations on zinc coated steel sheet at 20 mN load. (b) Image of matrix of Knoop indents and (c) the height profile and size of the Knoop indents at the cross section of the zinc coating at 20 mN load.

Table 2
Yield criteria parameters for zinc coating on steel sheet.

KHN-orientation	Value [kgf/mm^2]	Yield criteria parameters	Value
KHN_{i_a}	44.7	R_0^{bulk}	–
KHN_{i_b}	68.2	R_{90}^{bulk}	–
KHN_{i_c}	68.0	σ_y [41,50]	55–115 MPa
KHN_{i_d}	43.9	R_0^{KHN}	0.45
KHN_{i_e}	64.9	R_{90}^{KHN}	1.56
KHN_{i_f}	83.4	σ_y^{KHN}	57.7–81.7 MPa

substrate, individual grain orientation and grain boundaries (see Fig. 13b and c). The anisotropy determined using Knoop indentation accounts for the anisotropy in the zinc coating attributed to the *hcp* crystal structure of the zinc as well as the deformation textures induced in the zinc coating by the temper rolling of the galvanized steel sheet.

Initially the yield locus for the KHN data is plotted in the deviatoric plane as shown in Fig. 14. The points on the deviatoric plane are plotted along the lines following the stress ratios from equation (3.1) ($\alpha = \boldsymbol{B}$) and scaled according to the KHN data. Comparing the yield locus of the DC04 steel and the zinc coating from Figs. 11 and 14, it can be said the zinc coating has higher induced anisotropy compared to the DC04 steel sheet. The anisotropy in the plastic deformation of the zinc coating and the steel is induced from the rolling process. The difference in the size and amount of zinc along the thickness and surface plane could also be attributed to the anisotropy in the mechanical properties of zinc coatings. Additional anisotropy is inherent to the zinc grains due to their hcp (hexagonal closed pack) crystal structure. The difference in the critical resolved shear stress for the various slip systems in the zinc grains, *e.g.* basal slip, pyramidal slip and twinning results in its anisotropy [41,49].

After validating the yield locus obtained from the Knoop indentations of DC04 steel sheet with the bulk tests, the yield locus of zinc coating on steel sheets has been characterised by Knoop indentation. The KHN data has been listed for the 6 orientations in Table 2. The points are plotted in the plane stress $\sigma_1 - \sigma_2$ plane taking initial values of $R_0 = R_{90} = 1$ in Fig. 15. The values of R_0, R_{90} and σ_y are then varied (increased/decreased) using constants a and b as shown in the algorithm in Fig. 3. The distance d between the measured KHN-data points on the plane stress plane and the yield locus based on R_0, R_{90} and σ_y is computed. Finally, the optimized yield locus for the zinc coating on the steel sheet is plotted by optimizing the KHN-data points in Fig. 15. The parameters of the yield locus obtained using the procedure above are listed in Table 2.

Using equations (2.2) and (2.5) the parameters for the Hill's quadratic yield criteria of the zinc coating can be obtained from the R values

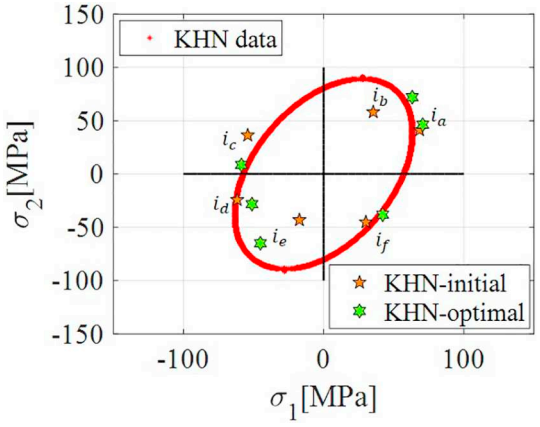

Fig. 15. The yield loci obtained from KHN data on the plane-stress plane optimized for anisotropy on zinc coating on steel sheet.

as $F = 0.2$, $G = 0.69$, $H = 0.31$. The values of F, G and H are implemented in the Hill's quadratic equation in principal stress coordinates given in equation (1.3). The constants of the shear stress in the Hill's quadratic equation in equation (1.1) are taken $N = 1.5$, $M = 1.5$ and $L = 1.5$ assuming isotropy. As of now the value of R_{45} (Lankford coefficient/strain ratio at 45° orientation) is required to obtain the value of N has not been obtained from the Knoop indentation method listed above.

The objective of the current work is developing a new indentation based method to characterize the yield locus for metallic coatings with rolling induced anisotropy. To elaborate on this method, as an example hot dip galvanized, temper rolled zinc coating have been used. The yield locus of the zinc coating has been successfully plotted from Knoop hardness data using the above method after an initial validation of the yield locus by Knoop indentation with the yield locus by standard tests for an uncoated cold rolled DC04 steel specimen.

4. Conclusion

To conclude, a method to obtain the yield parameters and to plot the anisotropic yield locus based on Knoop indentation has been developed. The yield parameters are optimized to plot the best fit yield locus from the KHN data. The method has been implemented to plot the yield locus for DC04 steel sheet and validated against bulk tests. Both experimental characterization procedures have been shown to be in good agreement. The method has been extended to plot the yield locus of the zinc coating on steel sheet. The parameters for the Hill's quadratic yield criteria have been derived from the plotted yield locus of the zinc coating and can be used in modelling of material deformation behaviour in various numerical simulations.

Declaration of competing interest

None.

Acknowledgment

This research was carried out under project number S22.1.14520a in the framework of the Partnership Program of the Materials innovation institute M2i (www.m2i.nl) and the Technology Foundation TTW (www.stw.nl), which is part of the Netherlands Organization for Scientific Research (www.nwo.nl) with project/grant number S22.1.14520a. The authors would also like to thank ing. Erik de Vries from the University of Twente for setting the Knoop indenter in the indentation set-ups, Dr. ir. Mohammad Bazrafshan from University of Twente for discussions on the optimization algorithm and TATA steel Europe R&D, Ijmuiden for the provision of the data and parameters for the yield loci of the DC04 steel sheets.

References

[1] S. Suwas, R.K. Ray, Deformation textures, Crystallographic Texture of Materials, Engineering, Materials and Processes, Springer, London, 2014, pp. 95–141.
[2] R. Hill, A theory of the yielding and plastic flow of anisotropic metals, Proceedings of the Royal Society of London Series A. Mathematical and Physical Sciences, vol. 193, 1948, pp. 281–297.
[3] R.V. Mises, Mechanik der festen Körper im plastisch-deformablen Zustand. Nachrichten von der Gesellschaft der Wissenschaften zu Göttingen, Mathematisch-Physikalische Klasse (1913) 582–592 1913 http://eudml.org/doc/58894.
[4] H. Tresca, Mémoire sur l'écoulement des corps solides soumis à de fortes pressions, C. R. Acad. Sci. Paris 59 (1864) 754.
[5] W.F. Hosford, A generalized isotropic yield criterion, J. Appl. Mech. 39 (1972) 607–609, https://doi.org/10.1115/1.3422732.
[6] R. Hill, Theoretical plasticity of textured aggregates, Mathematical Proceedings of the Cambridge Philosophical Society, vol. 85, Cambridge University Press, 1979, pp. 179–191.
[7] H. Vegter, P. Drent, H. Huetink, A planar isotropic yield criterion based on mechanical testing at multi-axial stress states, Proceedings of the Fifth International Conference on Numerical Methods in Industrial Forming Processes, 1995, pp. 345–350 Ithaca, New York.

[8] H. Vegter, A.H. van den Boogaard, A plane stress yield function for anisotropic sheet material by interpolation of biaxial stress states, Int. J. Plast. 22 (2006) 557–580, https://doi.org/10.1016/j.ijplas.2005.04.009.

[9] F. Barlat, J.W. Yoon, O. Cazacu, On linear transformations of stress tensors for the description of plastic anisotropy, Int. J. Plast. 23 (2007) 876–896, https://doi.org/10.1016/j.ijplas.2006.10.001.

[10] H. Vegter, C.H.L.J. ten Horn, Y. An, E.H. Atzema, H. H Pijlman, A.H. van den Boogaard, H. Huétink, Characterisation and modelling of the plastic material behaviour and its application in sheet metal forming simulation, in: E. Oñate, D.R.J. Owen (Eds.), Proceedings of VII International Conference on Computational Plasticity COMPLAS VII, CIMNE, Barcelona, 2003.

[11] M. Rossi, F. Pierron, M. Štamborská, Application of the virtual fields method to large strain anisotropic plasticity, Int. J. Solids Struct. 97 (2016) 322–335, https://doi.org/10.1016/j.ijsolstr.2016.07.015.

[12] F. Pierron, M. Grédiac, The Virtual Fields Method: Extracting Constitutive Mechanical Parameters from Full-Field Deformation Measurements, Springer Science & Business Media, New York, NY, 2012.

[13] S.M. Kalkhoran, Characterization of Anisotropic Plasticity in Material Systems Using Modified Indentation-Based Techniques, PhD Thesis, Northeastern University, 9781267835628, 2012.

[14] A. Yonezu, Y. Kuwahara, K. Yoneda, H. Hirakata, K. Minoshima, Estimation of the anisotropic plastic property using single spherical indentation—an FEM study, Comput. Mater. Sci. 47 (2009) 611–619, https://doi.org/10.1016/j.commatsci.2009.10.003.

[15] A. Yonezu, K. Yoneda, H. Hirakata, M. Sakihara, K. Minoshima, A simple method to evaluate anisotropic plastic properties based on dimensionless function of single spherical indentation–Application to SiC whisker-reinforced aluminium alloy, Mater. Sci. Eng. A 527 (2010) 7646–7657, https://doi.org/10.1016/j.msea.2010.08.014.

[16] D. Tabor, The Hardness of Metals, Oxford university press, 9780198507765, 2000.

[17] F. Knoop, C.G. Peters, W.B. Emerson, A sensitive pyramidal-diamond tool for indentation measurements, J. Res. Natl. Bur. Stand. 23 (1939) 39.

[18] D.N. French, D.A. Thomas, Hardness anisotropy and slip in WC crystals, Trans. Metall.. Soc. AIME 233 (1965) 950–952.

[19] F.W. Daniel, C.G. Dunn, The effect of orientation on Knoop hardness of single crystals of zinc and silicon ferrite, Trans.: Am. Soc. Met. 41 (1949) 419–442 NAID: 10016191481.

[20] P.L. Rittenhouse, M.L. Picklesimer, Comparison of Pole Figure Data Obtained by X-Ray Diffraction and Microhardness Measurements on Zircaloy-2 (No. ORNL-P-1165; CONF-650210-3), Oak Ridge National Lab., TN, 1965.

[21] R.G. Wheeler, D.R. Ireland, Multiaxial plastic flow of Zircaloy-2 determined from hardness data, Electrochemical Technology (US) Absorbed by, J. Electrochem. Soc. 4 (1966) 313–317 BNWL-SA-180.

[22] D. Lee, S. Jabara, W.A. Backofen, The Knoop-hardness yield loci for two titanium alloys, Trans. Metall. Soc. AIME 239 (1967) 1476–1478.

[23] D. Lee, W.A. Backofen, An experimental determination of the yield locus for titanium and titanium-alloy sheet, Trans. Metall. Soc. AIME 236 (1966) 1077–1084.

[24] B.C. Wonsiewicz, W.W. Wilkening, A comparison of conventional and knoop-hardness yield loci for magnesium and magnesium alloys, Trans. Metall. Soc. AIME 245 (1969) 1313–1319.

[25] F. Larson, A. Zarkades, Properties of Textured Titanium Alloys (No. MCIC-74-20), Metals and Ceramics Information Center, Columbus OH, 1974(Accession Number: AD0781884), https://apps.dtic.mil/dtic/tr/fulltext/u2/781884.pdf accessed 7 July 2019.

[26] M. F Amateau, W.D. Hanna, Comparison of first quadrant yield loci for Ti-6Al-4V with those predicted by Knoop hardness measurements, Metall. Mater. Trans. A 6 (1975) 417–419, https://doi.org/10.1007/BF02667299.

[27] K.L. Murty, I. Charit, Texture development and anisotropic deformation of zircaloys, Prog. Nucl. Energy 48 (2006) 325–359, https://doi.org/10.1016/j.pnucene.2005.09.011.

[28] M. Nakatsuka, M. Nagai, Reduction of plastic anisotropy of zircaloy cladding by neutron irradiation, (I) Yield loci obtained from Knoop hardness, J. Nucl. Sci. Technol. 24 (1987) 832–838, https://doi.org/10.1080/18811248.1987.9735886.

[29] L. Riester, P.J. Blau, E. Lara-Curzio, K. Breder, Nanoindentation with a Knoop indenter, Thin Solid Films 377 (2000) 635–639, https://doi.org/10.1016/S0040-6090(00)01298-0.

[30] L. Riester, T.J. Bell, A.C. Fischer-Cripps, Analysis of depth-sensing indentation tests with a Knoop indenter, J. Mater. Res. 16 (2001) 1660–1667, https://doi.org/10.1557/JMR.2001.0230.

[31] A.E. Giannakopoulos, T. Zisis, Analysis of Knoop indentation, Int. J. Solids Struct. 48 (2011) 175–190, https://doi.org/10.1016/j.ijsolstr.2010.09.014.

[32] A.E. Giannakopoulos, T. Zisis, Analysis of Knoop indentation strain hardening effects, Int. J. Solids Struct. 48 (2011) 3217–3231, https://doi.org/10.1016/j.ijsolstr.2011.07.014.

[33] M.I. Simões, A.X. Martins, J.M. Antunes, N.A. Sakharova, M.C. Oliveira, J.V. Fernandes, Numerical simulation study of the Knoop indentation test, in: E. Oñate, D.R.J. Owen, D. Peric, B. Suárez (Eds.), XI International Conference on Computational Plasticity. Fundamentals and Applications (COMPLAS XI), 2011, pp. 287–294 Barcelona.

[34] M. Simões, J. Antunes, J. Fernandes, N. Sakharova, Numerical simulation of the depth-sensing indentation test with Knoop indenter, Metals 8 (2018) 885, https://doi.org/10.3390/met8110885.

[35] J. Zhang, M. Sakai, Geometrical effect of pyramidal indenters on the elastoplastic contact behaviors of ceramics and metals, Mater. Sci. Eng. A 381 (2004) 62–70, https://doi.org/10.1016/j.msea.2004.04.015.

[36] G.B. Ghorbal, A. Tricoteaux, A. Thuault, G. Louis, D. Chicot, Mechanical characterization of brittle materials using instrumented indentation with Knoop indenter, Mech. Mater. 108 (2017) 58–67, https://doi.org/10.1016/j.mechmat.2017.03.009.

[37] A. Datye, L. Li, W. Zhang, Y. Wei, Y. Gao, G.M. Pharr, Extraction of anisotropic mechanical properties from nanoindentation of SiC-6H single crystals, J. Appl. Mech. 83 (2016) 091003 1–7, https://doi.org/10.1115/1.4033790.

[38] G. Li, X.Y. Long, S.S. Cui, Q.W. Huang, Z.P. Chen, S.H. Tan, Influence of zinc coating on anisotropic mechanical properties of hot dip galvanized steel sheet DP600, J. Phys. Conf. Ser. 1063 (2018) 012164 1–6, https://doi.org/10.1088/1742-6596/1063/1/012164 IOP Publishing Ltd..

[39] N. Coni, M.L. Gipiela, A.S.C.M. D'Oliveira, P.V.P. Marcondes, Study of the mechanical properties of the hot dip galvanized steel and galvalume®, J. Braz. Soc. Mech. Sci. Eng. 31 (2009) 319–326, https://doi.org/10.1590/S1678-58782009000400006.

[40] W. Wen, A.A. Becker, W. Sun, Determination of material properties of thin films and coatings using indentation tests: a review, J. Mater. Sci. 52 (2017) 12553–12573, https://doi.org/10.1007/s10853-017-1348-3.

[41] Y.T. Pei, G.M. Song, W.G. Sloof, J.T.M. De Hosson, A methodology to determine anisotropy effects in non-cubic coatings, Surf. Coat. Technol. 201 (2007) 6911–6916, https://doi.org/10.1016/j.surfcoat.2006.11.044.

[42] K. Ikegami, Experimental plasticity on the anisotropy of metals, Mechanical behaviour of Anisotropic Solids/Comportment Méchanique des Solides Anisotropes, Springer, Dordrecht, 1982, pp. 201–242.

[43] W.F. Hosford, Texture strengthening, Met. Eng. Quart. 6 (1966) 13–19 ISSN 0026-0967.

[44] D. Banabic, Anisotropy of sheet metal, in: D. Banabic, K. Pöhlandt (Eds.), Formability of Metallic Materials: Plastic Anisotropy, Formability Testing, Forming Limits, Engineering Materials, Springer, Berlin, Heidelberg, 2000, pp. 119–172.

[45] W.C. Oliver, G.M. Pharr, An improved technique for determining hardness and elastic modulus using load and displacement sensing indentation experiments, J. Mater. Res. 7 (1992) 1564–1583, https://doi.org/10.1557/JMR.1992.1564.

[46] A.C. Fischer-Cripps, Depth-sensing indentation testing, Introduction to Contact Mechanics, Mechanical Engineering Series, Springer, Boston, MA, 2007, pp. 189–199.

[47] A.C. Fischer-Cripps, Nanoindentation Test Instruments. In Nanoindentation, Springer, New York, NY, 2004, pp. 178–194.

[48] Y.G. An, E. Atzema, M. Workel, H. Vegter, L. Elliott, J. Moerman, A Comparison of Yield loci measured with mechanical tests and calculated from crystal plasticity for steel sheets, 1st International Conference on Super-high Strength Steels, 2005 Rome.

[49] R. Parisot, S. Forest, A.F. Gourgues, A. Pineau, D. Mareuse, Modeling the mechanical behavior of a multicrystalline zinc coating on a hot-dip galvanized steel sheet, Comput. Mater. Sci. 19 (2000) 189–204, https://doi.org/10.1016/S0927-0256(00)00155-5.

[50] G.M. Song, J.T.M. De Hosson, W.G. Sloof, Y.T. Pei, Evaluation of interface adhesion of hot-dipped zinc coating on TRIP steel with tensile testing and finite element calculation, WIT Trans. Eng. Sci. 91 (2015) 3–14, https://doi.org/10.2495/SECM150011.

[51] D.B. Marshall, T. Noma, A.G. Evans, A simple method for determining elastic-modulus–to-hardness ratios using Knoop indentation measurements, J. Am. Ceram. Soc. 65–10 (1982) c175–176, https://doi.org/10.1111/j.1151-2916.1982.tb10357.x.